Pergamon

Geochimica et Cosmochimica Acta, Vol. 66, No. 7, pp. 1185–1196, 2002

0016-7037/02 $22.00 + .00

PII S0016-7037(00)00849-3

Tetrad effect in rare earth element distribution patterns: A method of quantification with application to rock and mineral samples from granite-related rare metal deposits

T. Monecke,[1,*] U. Kempe,[1] J. Monecke,[2] M. Sala,[1] and D. Wolf[1]

[1]Institute of Mineralogy, Freiberg University of Mining and Technology, Brennhausgasse 14, 09596 Freiberg, Germany
[2]Institute of Theoretical Physics, Freiberg University of Mining and Technology, Bernhard von Cotta Straβe 4, 09596 Freiberg, Germany

(*Received May* 22, 2001; *accepted in revised form October* 5, 2001)

Abstract—In some geological environments, the tetrad effect can be observed as a split of rare earth element (REE) patterns into four rounded segments. A new method is proposed to quantify the sizes of the individual segments, and for the first time, the significance of observed tetrad effects is evaluated by taking analytical errors into account. The outlined method was applied to lanthanide patterns of whole-rock and fluorite samples collected from granite-related rare metal deposits. The REE patterns of the granite and greisen samples investigated exhibit significant tetrad effects that may not be accounted for by analytical uncertainties. It is shown that the study of whole-rock samples is insufficient to determine whether this effect is developed during fractional crystallization or is due to other processes such as fluid–rock interaction. A concave tetrad effect mirroring the pattern of the whole-rock samples was not observed in the REE patterns of related vein fluorite samples. Therefore, it is unlikely that the convex tetrad effect in the samples from the magmatic environment can be explained by removal of a respective complementary REE pattern by a coexisting hydrothermal fluid, as previously suggested. It is proposed that the tetrad effect formed within the magma–fluid system before emplacement in the subvolcanic environment where phase separation caused a split of this system into fluid and magma subsystems. Alternatively, the tetrad effect may also be inherited from an external fluid influencing the system during or after the emplacement of the magma. On the basis of the fluorite data, it is shown that the behavior of Eu in the fluids is not related to the tetrad effect. Consequently, different physico-chemical factors control the occurrence of both phenomena. Y was found to be strongly enriched in samples precipitating from hydrothermal fluids that experienced prolonged interaction with the wall-rocks, whereas the tetrad effect in the fluids vanished with time and increasing distance from the ore-bearing granite. Thus, these different geochemical parameters can be used to reconstruct different aspects of the fluid evolution within this type of deposit. *Copyright © 2002 Elsevier Science Ltd*

1. INTRODUCTION

The geochemistry of the rare earth elements (REEs) has been intensively studied in the past decades, and it has been found that the behavior of the REEs in most geological environments can be accounted for by differences in their ionic radii (increasing contraction of the 5s and 5p electron shells with increasing atomic mass) as well as variations in valence states (Ce^{3+} or Ce^{4+}, Eu^{2+} or Eu^{3+}). However, an additional feature in the distribution patterns of the REEs is the tetrad effect. This effect can cause a split of chondrite-normalized REE patterns into four rounded segments called tetrads (first tetrad, La-Ce-Pr-Nd; second tetrad, (Pm)-Sm-Eu-Gd; third tetrad, Gd-Tb-Dy-Ho; fourth tetrad, Er-Tm-Yb-Lu). The rounded segments are either convex or concave and form M-shaped and W-shaped lanthanide distribution patterns, respectively (Masuda et al., 1987).

The tetrad effect was initially observed in patterns of liquid–liquid REE distribution coefficients, and subtle interelement variations resembling this effect have been subsequently documented by various experimental studies and theoretical considerations (Bandurkin, 1964; Peppard et al., 1969; Jørgensen, 1970; Nugent, 1970; Siekierski, 1971; Kawabe, 1992; Kagi et al., 1993; Bau, 1999; Schijf and Byrne, 1999; Luo and Byrne, 2000). The existence of the tetrad effect in geological materials has been a matter of debate (Yurimoto et al., 1990; McLennan, 1994). Subtle tetrad effects have been recorded in the lanthanide patterns of seawater, marine precipitates, clastic sedimentary rocks, and various minerals (Masuda and Ikeuchi, 1979; Akagi et al., 1993, 1998; Liu et al., 1993; Kawabe, 1996; Kawabe et al., 1998). The pronounced convex tetrad effects recently recognized in samples from evolved granite systems provide the best available evidence that this effect indeed occurs in natural samples (Masuda and Akagi, 1989; Cocherie et al., 1991; Förster and Tischendorf, 1994; Höhndorf et al., 1994; Lee et al., 1994; Kawabe, 1995; Bau, 1996; Irber, 1999).

To study the existence and geochemical significance of the tetrad effect, the size of this effect has to be quantified. Masuda et al. (1994) and Minami and Masuda (1997) proposed methods of quantification that are based on the assumption that the four observed rounded tetrads can be approximated by four quadratic functions. The corresponding quadratic coefficients were employed as measures for the size of the tetrad effect. Irber (1999) pointed out that this fitting of observed REE patterns by using a least-squares method idealizes the existing tetrad effect by assuming an absence of any analytical deficiencies. Therefore, Irber (1999) proposed an alternative procedure for quantification. However, analytical errors were also not taken into account in this approach. In the present contribution, a method

*Author to whom correspondence should be addressed (tmonecke@mineral.tu-freiberg.de).

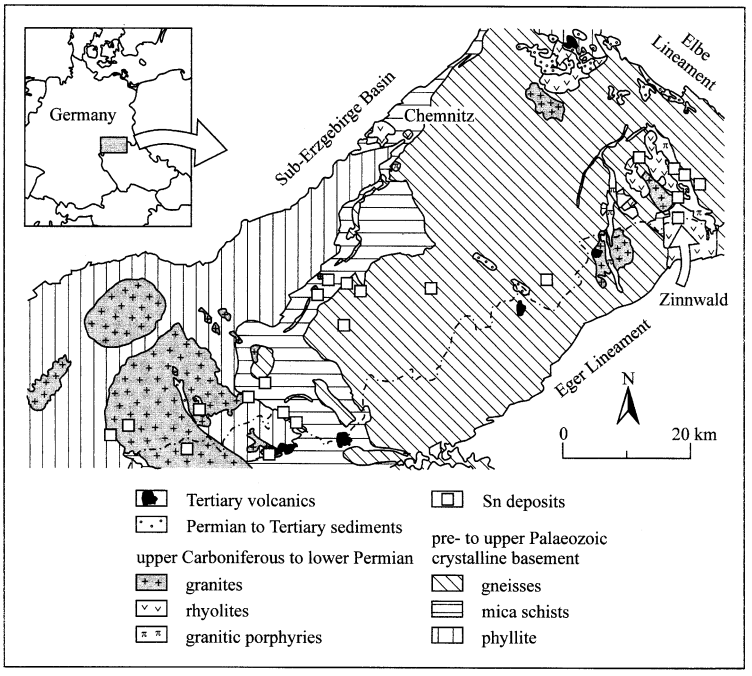

Fig. 1. Simplified geological map of the Erzgebirge Sn province, Germany, showing the distribution of late Herzynian granites and related Sn deposits as well as the setting of the Zinnwald deposit.

is given that allows a rapid quantification of the size of the tetrad effect in the individual rounded segments and additionally takes analytical errors into account.

On the basis of considerations by Masuda et al. (1987) and Kawabe (1995), many workers have accepted that the pronounced convex (M-shaped) tetrad effect in granite samples represents a residual REE pattern subsequent to extraction of a mirroring concave (W-shaped) tetrad effect by a coexisting fluid. Furthermore, it has been proposed that geochemical indicators such as the tetrad effect, the Eu anomaly, and the Y/Ho fractionation develop in parallel with granite evolution (Irber, 1999). To test the applicability of the previous models explaining the tetrad effects in granite-related rare metal deposits, the new method of quantification has been applied to tetrad effects in lanthanide patterns of whole-rock samples from the Zinnwald granite-related Sn deposit, Germany, and to lanthanide distribution patterns of fluorite samples that precipitated from related hydrothermal fluids. Quantification of the tetrad effect in fluorite samples from the Qaraoba, Aqshatau, and Kent granite-related rare metal deposits, Kazakhstan, was performed to determine whether the tetrad effect and the anomalous behavior of Eu and Y are indeed linked to a single process occurring during the evolution of mineralizing hydrothermal fluids.

2. GEOLOGICAL BACKGROUND AND SAMPLE DESCRIPTION

2.1. Zinnwald Tin Deposit (Germany)

The Zinnwald Sn deposit is situated at the border between the Czech Republic and Germany and forms part of the late Herzynian tin province of the Erzgebirge (Fig. 1). The geology and geochemistry of the tin deposit have been discussed by Štemprok (1967), Štemprok and Šulcek (1969), Cocherie et al. (1991), and Rub et al. (1998). The Li-F granite of Zinnwald is an elongated body that is hosted by the Teplice rhyolite. Greisen bodies, flat-lying ore veins, and some steeply dipping ore veins are hosts to the mineralization. These mineralized cassiterite–quartz veins occur within the endo- and exocontact of the granite. For the purpose of quantification of the tetrad effect, samples from the Teplice rhyolite, kaolinized and sericitized albite granite samples, and greisen samples have been analyzed. A representative least-altered rhyolite (sample MR 14) was collected ~50 m away from the granite contact, and an intensely altered rhyolite (sample MR 15) was taken ~35 m from the granite contact. The least-altered sample, MR 14, showed only minor replacement of feldspar by kaolinite and sericite, whereas the altered rhyolite MR 15 contained substantial amounts of blue violet colored fluorite. The analyzed albite granite samples are medium to coarse grained and variably altered. Albite is typically replaced by sericite and kaolinite. The albite granite MGt 38 was sampled close to the contact of the granite with the Teplice rhyolite, whereas the sample MGt 53 was taken from albite granite adjacent to a flat-lying ore vein. The greisen samples are medium to coarse grained and contain variable amounts of topaz, zinnwaldite, and lepidolithe. Sample MGr 33 is a topaz greisen, and sample MGr 43 is an example of mica greisen from the Zinnwald deposit. In addition to the whole-rock samples, three fluorite separates were prepared. The fluorite samples ZW315/2g (green core) and ZW315/2v (violet rim) were separated from a single zoned fluorite crystal collected from a flat-lying vein within the endocontact, whereas the fluorite ZW 379 (white violet) was taken from a flat-lying vein in the exocontact.

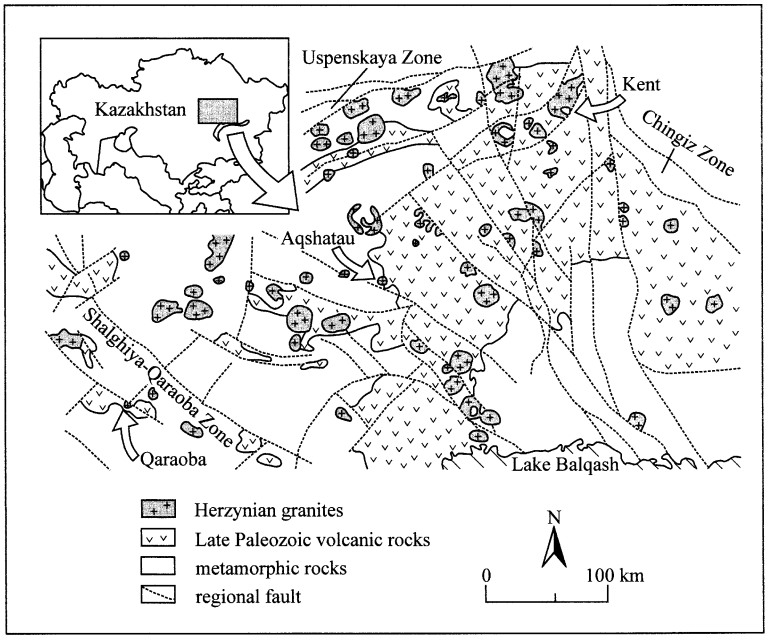

Fig. 2. Generalized geological map of central Kazakhstan showing the distribution of Herzynian granites as well as the geological setting of the granite-related rare metal deposits Qaraoba, Aqshatau, and Kent (Morozov et al., 1996).

2.2. Qaraoba, Aqshatau, and Kent Rare Metal Deposits (Kazakhstan)

Several fluorite samples were collected from the Qaraoba W deposit, the Aqshatau Be-Mo-W deposit, and the Kent Nb-Zr-REE deposit. These deposits formed in relation to granite intrusions within the Herzynian rare metal province of central Kazakhstan (Fig. 2). The spectroscopic behavior of the fluorite samples investigated in the present contribution are reported by Morozov et al. (1996).

The Qaraoba W deposit is located within the apical part of a Li-F granite body. Greisen bodies and quartz–wolframite veins occur in the endocontact of the granite and represent the principal hosts to the mineralization. However, fluorite–quartz ore bodies with wolframite are also hosted by marble in the Solnechnoe ore field to the west of the granite intrusion (Morozov et al., 1996, and references therein). Early fluorite occurring in the quartz–wolframite veins from Qaraoba has a brown color and forms cloudy cores (sample KO 40a) within green fluorite aggregates (sample KO 40b). Green fluorite (sample KO 1g) also forms rims surrounding green violet fluorite. Fluorite from the Solnechnoe ore field is commonly brown (sample SN 309a).

The Aqshatau deposit comprises complex W-Mo-Be mineralized zones that formed in relation with a Li-F granite. The Li-F granite intruded into granite, sedimentary, and volcanic rocks and is partly exposed at the surface (Beskin et al., 1996). The main ore minerals (wolframite, molybdenite, beryl, and bismuth minerals) occur in quartz–topaz and quartz–wolframite greisen bodies as well as in quartz veins. Early fluorite is bluish, reddish rose, or rose and occurs together with wolframite, beryl, and sulfides in quartz–topaz greisen bodies (bluish violet fluorite sample AC 16404v), quartz–sericite altered rocks, and quartz veins (reddish brown fluorite AC 2 and rose fluorite AC 16038r). Late green (sample AC 16038g) and violet fluorite often forms zones that have overgrown the early-formed fluorite crystals.

The granite pluton of the Kent Nb-Zr-REE deposit intruded into volcanic and sedimentary rocks. The pluton forms three intrusive complexes that cover a surface outcrop of ~650 km^2. The mineralization occurs in intensely altered pegmatite bodies and veins within the endocontact of the granite (Zakharchenko et al., 1968). Barren pegmatite bodies in the endocontact commonly carry optical fluorite. A Nb-Zr-REE–bearing altered pegmatite body was found to contain dark violet fluorite (sample KN 3), whereas weakly mineralized and barren pegmatite bodies are host to early emerald green (KN 6) and younger light colored pale rose, grayish blue, and colorless (sample KN 1a) fluorite. Late-stage fluorite is pale green (samples KN 2a) or violet.

3. ANALYTICAL METHODS

Initially, the whole-rock samples were crushed and powdered in an agate mortar. Sample powders (100 mg) were decomposed in polyterafluoroethylene (PTFE) pressure containers by means of a combined HF/$HClO_4$ acid digestion procedure (Dulski, 1994, 2001). After digestion, the samples were evaporated to incipient dryness and redissolved with HCl. The final sample dissolution was performed with HCl because the high field strength elements are stabilized in solution in this way (Münker, 1998; Robinson et al., 1999; Yu et al., 2000; Dulski, 2001). Before analysis, Ru and Re solutions were added as internal standards to compensate for instrumental drift. Inductively coupled plasma (ICP) mass spectrometry (MS) analysis of the obtained sample solutions was carried out with an externally calibrated Perkin-Elmer ELAN 5000A quadrupole ICP mass spectrometer. Details on the interference corrections

applied to correct analyte isotopes for molecular and isobaric interferences are given by Dulski (1994, 2001). The analytical procedure was validated by repeated independent sample preparation and analysis of international reference standards. The relative deviations of the standard analyses to the reference values are typically well below ±10% (Dulski, 1994, 2001; Irber, 1999).

The fluorite samples were hand-picked and subsequently powdered in an agate mortar. The fluorite powders were decomposed in a platinum vessel by a $HF/HClO_4$ acid digestion procedure. After evaporation to dryness, the residue was dissolved in HCl. The obtained solutions were utilized for cation exchange separation of the REEs and Y from matrix elements via a method slightly modified from Watkins and Nolan (1992). Chromatographic glass columns fitted with glass wool and PTFE stopcocks were charged with 200 to 400 mesh DOWEX 50W-X8 cation resin. The loading and eluating solutions were fed through the columns at an average flow rate of 1.5 mL min^{-1}. After equilibrating the ion-exchange resin with HCl, the sample solutions were loaded onto the columns. Unwanted elements were eluted with HCl, then HNO_3. Both eluates were discarded. The REEs + Y were eluted with HNO_3/oxalic acid, then HNO_3. The combined eluates were evaporated to dryness and redissolved in 10 mL HNO_3. Trace element measurements were carried out by ICP-AES with a Perkin-Elmer ICP-AES Plasma 1000. The precision and accuracy of the ICP-AES analysis were determined by using in-house and international fluorite reference standards. The deviations of the analytical results from recommended values were found to be in the order of ±10% or below (Goldstein, 1997).

4. QUANTIFICATION OF THE SIZE OF THE TETRAD EFFECT AND TEST OF SIGNIFICANCE

The methods of quantification proposed in the present contribution were designed for normalized REE patterns that exhibit a split into four rounded segments of logarithmically expressed concentrations. The size of the tetrad effect in these patterns is best determined separately for each tetrad. To distinguish the four segments of a REE pattern showing the tetrad effect, the tetrads are consecutively numbered as $i = 1 \ldots 4$.

The tetrad effect can be treated similarly to the quantification of Ce or Eu anomalies in logarithmic representations and is given as

$$t_i = \sqrt{\frac{x_{Bi}x_{Ci}}{x_{Ai}x_{Di}}} \quad (1)$$

where x_{Ai} is the chondrite-normalized concentration of the first element in tetrad i, x_{Bi} and x_{Ci} are the concentrations of the central elements, and x_{Di} is the chondrite-normalized concentration of the last element in the tetrad. The value of t_i is larger than one for a convex tetrad in a logarithmic plot, equal to one if the elements plot on a straight line, and smaller than one for a concave tetrad. Eqn. 1 is equivalent to the method of quantification proposed by Irber (1999). The first branch should not be quantified if Ce exhibits anomalous behavior. The second branch cannot be used for quantification at all because Pm does not occur in nature. In some cases, quantification of the tetrad effect may therefore only be possible for the third and fourth segments of REE patterns.

However, the size of the tetrad effect of a single tetrad in the logarithmic REE plot is better described by the mathematically more meaningful relative standard deviation of the chondrite-normalized concentrations of the two central elements (x_{Bi} and x_{Ci}) within the tetrad from a straight line that connects the contents of the first (x_{Ai}) and the last element (x_{Di}). The relative standard deviation T_i in a logarithmic plot is given by

$$T_i = \sqrt{\frac{1}{2} \times \left(\left[\frac{x_{Bi}}{(x_{Ai}^{2/3}x_{Di}^{1/3})} - 1 \right]^2 + \left[\frac{x_{Ci}}{(x_{Ai}^{1/3}x_{Di}^{2/3})} - 1 \right]^2 \right)}. \quad (2)$$

T_i is zero if the four elements plot on a straight line whereas $T_i > 0$ if the branch is either convex or concave. T_i can also be multiplied with 100% to give the deviation as a percentage.

To get one single characteristic, the values of T_i^2 determined on $N = 2$ or 3 individual tetrads can be averaged to yield an overall value of T according to

$$T = \sqrt{\frac{1}{2N} \times \sum_{i=1}^{N} \left(\left[\frac{x_{Bi}}{(x_{Ai}^{2/3}x_{Di}^{1/3})} - 1 \right]^2 + \left[\frac{x_{Ci}}{(x_{Ai}^{1/3}x_{Di}^{2/3})} - 1 \right]^2 \right)}. \quad (3)$$

The value of T should be calculated from all three tetrads (La-Nd, Gd-Ho, Er-Lu) but can also be determined from the last two tetrads if anomalous Ce behavior hampers the calculation of the first tetrad. The value of T is statistically a more meaningful index than the geometric mean t determined from three (or two) t_i values as proposed by Irber (1999).

The values of t_i and T_i can be used to show that an apparent tetrad effect does not result from analytical errors occurring during the REE determination. From Taylor expansions of Eqns. 1 and 2, it follows that the calculated values of t_i and T_i have to fulfill the following inequalities to indicate that the tetrad effect is significant:

$$t_i \gtrless 1 \pm \frac{1}{2} \times [d_{Ai} + d_{Bi} + d_{Ci} + d_{Di}], \quad (4)$$

and

$$T_i > \sqrt{\frac{1}{2} \times \left[\frac{5}{9}d_{Ai}^2 + d_{Bi}^2 + d_{Ci}^2 + \frac{5}{9}d_{Di}^2 + \frac{4}{3}d_{Ai}d_{Bi} + \frac{2}{3}d_{Ai}d_{Ci} + \frac{8}{9}d_{Ai}d_{Di} + \frac{2}{3}d_{Bi}d_{Di} + \frac{4}{3}d_{Ci}\,d_{Di} \right]^{1/2}}, \quad (5)$$

respectively, where

$$d_{Ai} = \frac{|\Delta x_{Ai}|}{x_{Ai}};\ d_{Bi} = \frac{|\Delta x_{Bi}|}{x_{Bi}};\ d_{Ci} = \frac{|\Delta x_{Ci}|}{x_{Ci}};\ d_{Di} = \frac{|\Delta x_{Di}|}{x_{Di}}$$

are the analytical errors. In the case of the ICP-MS and ICP-AES determinations of the lanthanides in whole-rock and fluorite samples, the analytical errors are estimated to be below ±10% (see above). Significant tetrad effects should therefore have T_i values exceeding 0.2, whereas the t_i values have to be below 0.8 for concave and higher than 1.2 for significant convex tetrad effects.

The test of significance of the tetrad effect should be performed separately for each tetrad because the overall value T does not provide a meaningful measure for such a test. For instance, lanthanide patterns may lack a chondrite-normalized

Table 1. REE and Y data of representative whole-rock and fluorite samples from the Zinnwald deposit.[a]

	Rhyolite		Albite granite		Greisen		Fluorite		
Element	MR 14	MR 15	MGt 38	MGt 53	MGr 33	MGr 43	ZW 315/2g	ZW 315/2v	ZW 379
Y	50	62	17	20	4	15	374	152	60.6
La	64.9	52.8	11.0	16.2	4.09	12.6	115	21.8	14.2
Ce	133	114	33.0	48.1	11.6	37.2	316	—	32.2
Pr	15.6	14.0	4.13	5.65	1.30	4.43	38.6	11.0	3.53
Nd	51.5	46.9	10.6	14.5	3.07	10.8	131	39.3	15.3
Sm	10.4	11.2	3.21	4.35	0.759	3.03	61.7	9.94	4.68
Eu	0.427	0.227	<0.05	<0.05	<0.05	<0.05	0.67	0.23	0.67
Gd	9.13	10.8	2.44	2.71	0.456	2.24	67.2	6.74	5.83
Tb	1.49	1.88	0.651	0.709	0.138	0.589	17.2	1.60	1.11
Dy	8.81	11.6	4.75	5.41	1.04	4.39	151	18.5	8.31
Ho	1.69	2.25	0.98	1.11	0.221	0.917	34.3	4.49	1.47
Er	4.87	6.75	3.61	4.25	0.873	3.48	105	17.8	6.30
Tm	0.702	1.07	0.790	0.971	0.217	0.814	25.5	4.47	—
Yb	4.64	7.31	6.71	8.20	1.88	6.98	188	30.5	8.02
Lu	0.662	1.03	1.07	1.34	0.320	1.13	25.4	4.46	1.24
La_n/Yb_n	9.68	5.00	1.14	1.37	1.51	1.25	0.42	0.49	1.23
Y_n/Dy_n	0.88	0.83	0.56	0.58	0.60	0.53	0.39	1.28	1.13
Eu/Eu*	0.13	0.06	—	—	—	—	0.03	0.09	0.39
T_1	0.11	0.14	0.52	0.51	0.54	0.55	0.26	—	0.06
T_3	0.03	0.06	0.27	0.26	0.33	0.25	0.19	0.18	0.18
T_4	0.01	0.05	0.16	0.17	0.20	0.19	0.33	0.32	—
T	0.07	0.09	0.35	0.35	0.38	0.37	0.27	—	—

[a] All data in parts per million; a dash indicates that the value was not determined. The normalization is based on the C1 chondrite data given by Anders and Grevesse (1989). The Eu anomaly is defined as $Eu/Eu^* = Eu_n/\sqrt{Sm_n \times Gd_n}$.

light REE ($LREEs_n$) tetrad effect but may show two tetrads in the normalized heavy REEs ($HREEs_n$). The resultant value of T may imply that the effect is not significant, although the two tetrads of the HREEs may not be accounted for by analytical difficulties. In principle, it also has to be taken into account that the values of T_i (and t_i) slightly depend on the choice of chondrite values used for normalization of the measured lanthanide concentrations. Inequalities 4 and 5 should therefore theoretically include terms derived from the uncertainty in the chondrite values. However, such a treatment would be impracticable because the errors of chondrite data sets taken from the literature cannot be readily determined.

It is recommended to test possible relationships between the size of the tetrad effect and other trace element concentrations or ratios as well as parameters like the size of the Eu anomaly in logarithmically scaled plots. As shown for several trace elements (Ahrens, 1966), the distribution function f(x) of one chondrite-normalized REE x in a large set of samples can typically be approximated by a log-normal distribution (the distribution function of the log values of x are then described by a normal distribution). The distribution function f(x) has a positive skewness because $x \geq 0$ with $f(x=0)=0$ and because the distribution has to have a long, thin upper tail toward the maximum value of x. The deviation from a log-normal distribution for any arbitrarily chosen positive skewed distribution function with $f(x=0)=0$ is insignificant even for several thousand samples. Assuming that the distribution functions of the x_{Ai}, x_{Bi}, x_{Ci}, and x_{Di} are best described by log-normal distributions, the resulting functions $f(T_i)$ and $f(t_i)$ are not such distributions because Eqns. 1 and 2 are nonlinear. However, because $T_i \geq 0$ and $t_i \geq 0$, the distribution functions are also positively skewed and can therefore be approximated by log-normal distributions.

5. RESULTS

5.1. Tetrad Effect in Whole-Rock and Fluorite Samples from the Zinnwald Tin Deposit

The tetrad effect in lanthanide patterns of rhyolite, albite granite, and greisen samples from the tin deposit Zinnwald was quantified by Eqns. 2 and 3. Lanthanide data of the representative whole-rock samples are listed in Table 1 together with the calculated sizes T_i and T of the tetrad effect. The corresponding chondrite-normalized REE patterns are given in Figure 3. The frequency distributions of the obtained T_i and T values are given in Figure 4.

The REE patterns of the rhyolite samples are characterized by decreasing chondrite-normalized concentrations from La to Lu and by pronounced negative Eu anomalies. Samples of the Teplice rhyolite show an absence of tetrad effects or very weak convex tetrad effects, with T_i values below the level of analytical significance. Therefore, it cannot be fully excluded that the weak tetrad effect in these samples may represent an analytical artifact. However, comparison of sample MR 15 with MR 14 (Fig. 3a) shows that alteration of the rhyolitic wall-rock by hydrothermal fluids related to the granite intrusion led to a small but systematic increase of the size of the tetrad effect in the three quantifiable tetrads, as well as an increase of the size of the negative Eu anomaly and enrichment of the $HREEs_n$. The albite granite and greisen samples have kinked REE patterns. The Eu content in the analyzed whole-rock samples was always found to be below the limit of detection (0.05 ppm). The

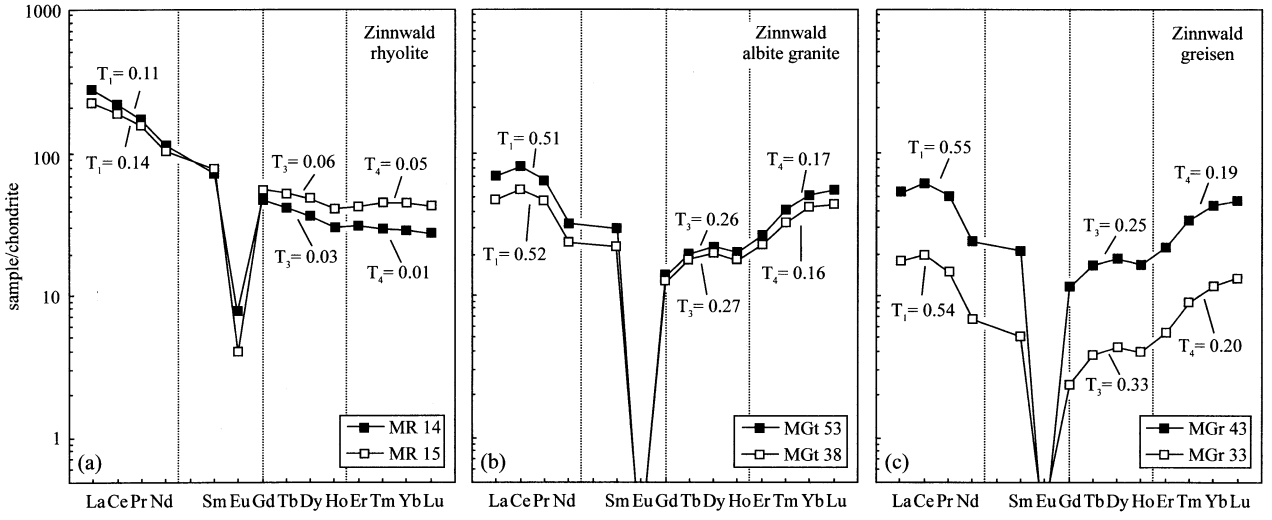

Fig. 3. Representative chondrite-normalized REE concentrations of (a) least-altered (sample MR 14) and pervasively altered (sample MR 15) Teplice rhyolite, (b) albite granite (samples MGt 38 and MGt 53), and (c) topaz greisen (sample MGr 33) and mica greisen (sample MGr 43) from the Zinnwald deposit. Note the increase in the $HREE_n$ concentrations and the size of the tetrad effect in the altered wall-rock rhyolite in comparison to its least-altered equivalent.

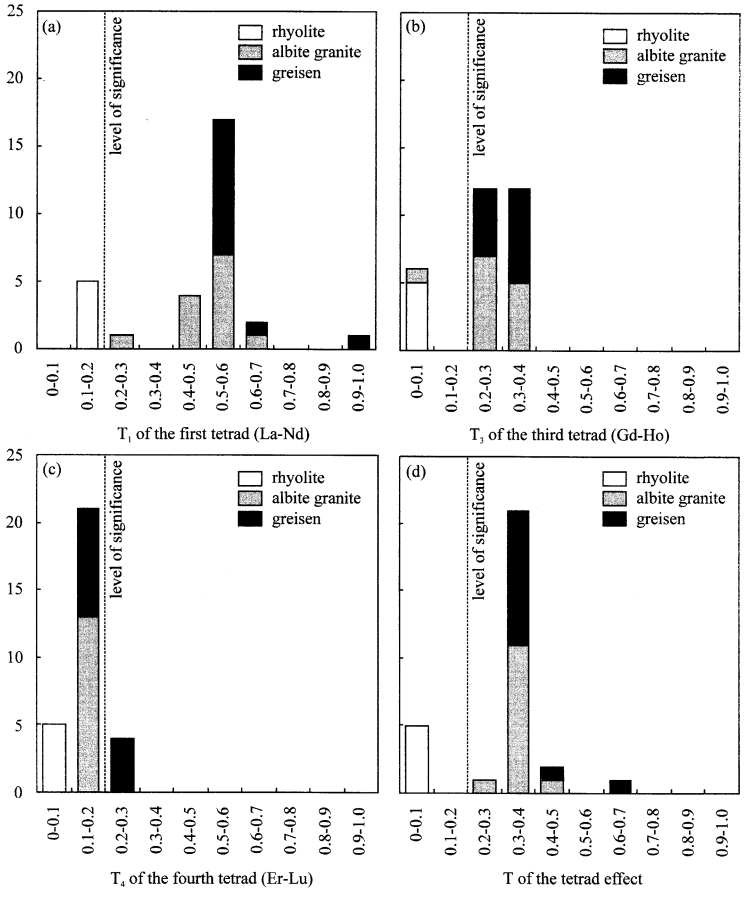

Fig. 4. Frequency distributions of the sizes of the tetrad effect T_1, T_3, T_4, and of the overall value T for all analyzed whole-rock samples from the Zinnwald deposit.

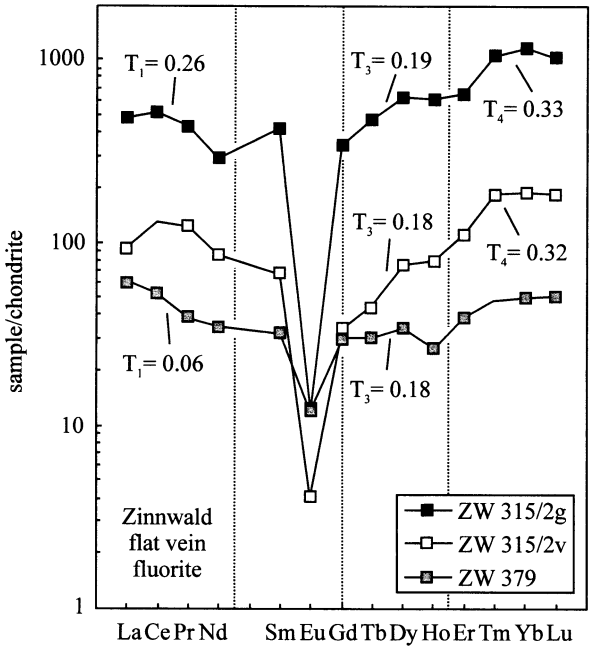

Fig. 5. Chondrite-normalized REE concentrations of the three analyzed fluorite samples from the Zinnwald deposit. The REE distributions in the fluorite samples ZW315/2g (green core) and ZW315/2v (violet rim) of a single zoned fluorite aggregate from the endocontact are distinctly different to the lanthanide distribution of the sample ZW 379 (white violet) from the exocontact.

sizes of the convex tetrads in the analyzed albite granite and greisen samples are more pronounced than in the Teplice rhyolite and commonly exceed the level of analytical significance (Figs. 3, 4). The individual rounded tetrads in the chondrite-normalized REE patterns have variable sizes, with the first tetrad being more strongly developed than the third and the fourth segments (Fig. 4).

The lanthanide data determined on the three fluorite samples from Zinnwald are listed in Table 1 along with the calculated T_i and T values. The REE patterns are given in Figure 5. The two zones of the fluorite aggregate sampled from a flat vein in the endocontact show a $HREEs_n$ enrichment and negative Eu anomalies. The $HREEs_n$ are more enriched in the green core than in the violet rim, and the negative Eu anomaly is more pronounced in the core of the zoned crystal (Fig. 5). The white violet sample ZW 379 from a flat vein in the exocontact shows an enrichment of $LREEs_n$ and an even smaller negative Eu anomaly. Total REE concentrations decrease from the endocontact samples ZW 315/2g and ZW 315/2v to the exocontact sample ZW 379. The sizes of the tetrad effect of the individual branches are similar in the two different colored fluorite zones ZW 315/2g and ZW 315/2v. The size of the tetrad effect is the highest in the fourth tetrad and lower in the first and third tetrads. The T_i values exceed the level of significance for the fourth and first convex tetrads. The tetrad effect of the first branch in the exocontact fluorite is less developed than in the endocontact samples and is below the level of significance. The Y_n/Dy_n ratio is low in the early sample, whereas the younger fluorite samples, ZW 315/2v and ZW 379, have Y_n/Dy_n ratios close to unity. The Y_n/Dy_n ratio is used instead of the Y/Ho ratio to identify an anomalous Y behavior because low Ho concentrations complicate precise determinations of this element in some HREE-depleted samples.

5.2. Tetrad Effect in Fluorite Samples from the Qaraoba, Aqshatau, and Kent Rare Metal Deposits

The data obtained on the fluorite samples from the rare metal deposits in Kazakhstan are listed in Table 2 together with the calculated T_i and T values. The normalized REE patterns of the fluorite samples are given in Figures 6 to 8.

Figure 6 shows that the fluorite samples from the endocontact of the Qaraoba W deposit are characterized by an enrichment of $HREEs_n$ over the $LREEs_n$ and distinct negative Eu anomalies. The $HREE_n$ enrichment is more pronounced in the early fluorite KO 40a than in the late samples KO 1g and KO 40b. In contrast, Eu anomalies are more pronounced in the late samples. The tetrad effects are weak and close to or below the level of significance and appear to decrease during the evolution of the hydrothermal fluids within the endocontact. The exocontact sample (fluorite SN 309b) from the Solnechnoe ore field exhibits a flat REE distribution pattern with a weak negative Eu anomaly. The third and fourth tetrads are well developed and exceed the threshold of significance. In the endocontact, the Y_n/Dy_n ratio increases from the early fluorite to the late stage samples. The exocontact sample is typified by a very low Y_n/Dy_n ratio.

In analogy to the Qaraoba fluorite samples, fluorite from the Aqshatau W-Mo-Be deposit is enriched in the $HREEs_n$ (Fig. 7). The $HREEs_n$ are more enriched in the early fluorite samples (samples AC 2, AC 16404v, and AC 16038r) than in the late fluorite AC 16038g. Eu anomalies are absent or weakly developed in early fluorite and are moderately negative in the late stage sample. The tetrad effect is very weak and below the level of significance. Only the third segment in the lanthanide pattern of the quartz–topaz greisen body sample (fluorite AC 16404v) was found to be significant. The Y_n/Dy_n ratios in the early samples AC 2 and AC 16404v are close to unity. A marked increase of the Y_n/Dy_n ratio is observed from the rose colored core (sample AC 16038r) to the green rim (sample AC 16038g) of the zoned fluorite aggregate investigated.

The samples from the Kent Nb-Zr-REE deposit show variable enrichments of the $HREEs_n$ and exhibit significant negative Eu anomalies (Fig. 8). The $HREE_n$ enrichment is most pronounced in the early fluorite KN 1a from the barren pegmatite whereas the samples KN 2a and KN 6 have significantly higher $LREE_n$ concentrations. With the exception of the violet fluorite sample KN 3 from the Nb-Zr-REE–bearing pegmatite, the tetrad effect in these samples is below the level of significance.

5.3. Relationship between Eu/Eu*, Y_n/Dy_n, and the Size of the Tetrad Effect in Fluorite REE Patterns

The changes in the sizes of the Eu anomaly and of the tetrad effect described above are generalized in an Eu/Eu* vs. T_3 plot given in Figure 9. The plot illustrates that there is no simple correlation between the tetrad effect and the size of the Eu anomalies in fluorite REE patterns. However, within a single deposit, increasingly negative Eu anomalies in fluorite patterns

Table 2. REE and Y data of representative fluorite samples from the Qaraoba, Aqshatau, and Kent deposits.[a]

	Qaraoba				Aqshatau				Kent			
Element	KO 1g	KO 40a	KO 40b	SN 309b	AC 2	AC 16038g	AC 16038r	AC 16404v	KN 1a	KN 2a	KN 3	KN 6
Y	160	135	109	7.07	274	60.0	721	24.8	307	169	80.1	384
La	1.70	—	—	—	—	—	—	—	—	25.0	29.3	750
Ce	7.05	4.37	8.00	7.74	34.3	7.42	4.72	1.86	1.48	42.7	91.6	1151
Pr	1.17	0.87	1.27	1.03	3.74	0.64	0.61	0.21	0.33	4.90	10.8	106
Nd	5.42	5.70	5.61	4.29	15.4	2.26	3.31	0.36	2.06	17.7	31.5	283
Sm	2.29	5.79	2.34	1.36	6.24	0.39	3.34	0.35	1.36	4.67	12.8	53.3
Eu	0.03	0.58	0.07	0.29	1.06	0.06	2.32	0.24	0.08	0.60	0.40	1.47
Gd	2.89	6.63	2.74	1.32	13.3	0.63	14.1	1.43	2.89	5.61	10.3	48.6
Tb	0.51	1.50	0.59	0.27	3.45	0.11	3.70	0.40	0.59	0.93	2.67	10.26
Dy	3.56	11.3	4.83	1.74	31.8	0.90	32.0	3.48	5.28	6.96	19.6	74.2
Ho	0.82	2.34	1.11	0.30	8.20	0.27	8.51	0.80	1.52	1.67	3.80	16.3
Er	3.08	9.16	4.20	0.92	33.8	1.15	33.7	2.96	5.88	5.96	13.3	58.1
Tm	0.58	2.08	0.80	0.17	6.90	0.22	6.18	0.60	0.91	1.00	2.35	9.83
Yb	5.24	21.5	6.96	1.39	60.2	2.08	56.1	5.42	6.90	8.08	17.8	76.9
Lu	0.82	3.70	1.09	0.17	11.6	0.45	10.5	1.02	1.05	1.40	2.77	11.1
Ce_n/Yb_n	0.36	0.05	0.31	1.50	0.15	0.96	0.02	0.09	0.06	1.42	1.39	4.03
Y_n/Dy_n	6.99	1.86	3.51	0.63	1.34	10.37	3.51	1.11	9.05	3.78	0.64	0.81
Eu/Eu*	0.04	0.28	0.08	0.66	0.35	0.37	1.03	1.03	0.12	0.36	0.11	0.09
T_1	0.33	—	—	—	—	—	—	—	—	0.05	0.46	0.08
T_3	0.03	0.17	0.09	0.21	0.12	0.15	0.11	0.23	0.07	0.09	0.29	0.09
T_4	0.11	0.15	0.10	0.24	0.02	0.07	0.04	0.03	0.03	0.03	0.06	0.08
T	0.20	—	—	—	—	—	—	—	—	0.06	0.31	0.08

[a] All data in parts per million; a dash indicates that the value was not determined. The normalization is based on the C1 chondrite data given by Anders and Grevesse (1989). The Eu anomaly is defined as $Eu/Eu^* = Eu_n / \sqrt{Sm_n \times Gd_n}$.

appear to be related to decreasing tetrad effects. This observation contradicts the relationship observed by Irber (1999) for whole-rock samples from ore-bearing granites. Moreover, a Y_n/Dy_n vs. T_3 plot for fluorite from the three deposits shows that there is no obvious correlation between Y fractionation and the size of the tetrad effect (Fig. 9) as described by Irber (1999). Irber and Bau (1995), Bau (1996), and Irber (1999) also mentioned that Y/Ho fractionation, similar to the Y_n/Dy_n trend observed for fluorite samples in the present study, may sometimes be observed for whole-rock geochemical data.

6. DISCUSSION

The convex tetrad effect in granite lanthanide patterns has been previously attributed to fractional crystallization during granite differentiation or, to a characteristic of magma–fluid systems that develops during granite crystallization under open conditions (Cocherie et al., 1991; McLennan, 1994; Kawabe, 1995; Irber, 1999). Irber (1999) showed that mineral fractionation is an unlikely reason for the development of the tetrad effect in granitic systems because the tetrad effect in whole-rock REE patterns could not be generated in Rayleigh fractionation calculations, even allowing for random mineral combinations. Therefore, Irber (1999) argued that the convex tetrad effect of granite samples must have resulted from interaction of the granitic melt with a coexisting fluid at a late stage of the granite crystallization after the magma–fluid system was split into magma and fluid subsystems. This assumption implies that the convex tetrad effect in the granite samples represents a residual lanthanide pattern after extraction of a mirroring concave tetrad pattern into a coexisting fluid that subsequently escaped from the magma–fluid system (Kawabe, 1995; Irber, 1999).

However, because the investigated hydrothermal precipitates (fluorite), including those collected from outside the granite bodies, do not show mirroring concave tetrad effects in their lanthanide patterns, the results obtained for the Zinnwald samples do not support the argument that the tetrad effect is indicative of open system conditions during crystallization. Moreover, the observed changes in the whole-rock lanthanide patterns of rhyolite during hydrothermal alteration, as well as the pronounced tetrad effect in the greisen samples, also lend no support to previous conclusions that hydrothermal fluids escaping from magmatic systems exhibit concave tetrad effects. Therefore, it appears more likely that the tetrad effect in the magma–fluid system developed before the shallow intrusion in the subvolcanic environment where the magma–fluid system was split into magma and fluid subsystems. Alternatively, the tetrad effect of the whole-rocks may have been inherited from a fluid phase during or after emplacement of the magma. In this context, it is important to note that not only the greisen samples from Zinnwald, but also all investigated granite samples are intensely altered. Therefore, the geochemistry of the whole-rock samples may not directly reflect the lanthanide pattern of the melt at the time of granite crystallization.

It has been well established that REE patterns of fluorite closely resemble that of the fluorite precipitating fluid and that tetrad effects in fluorite REE patterns cannot be accounted for by fluid/mineral fractionation (Marchand et al., 1976; Grappin et al., 1979). Consequently, in contrast to the investigated whole-rocks, the geochemistry of fluorite samples allows direct reconstruction of the chemistry of hydrothermal fluids escaping

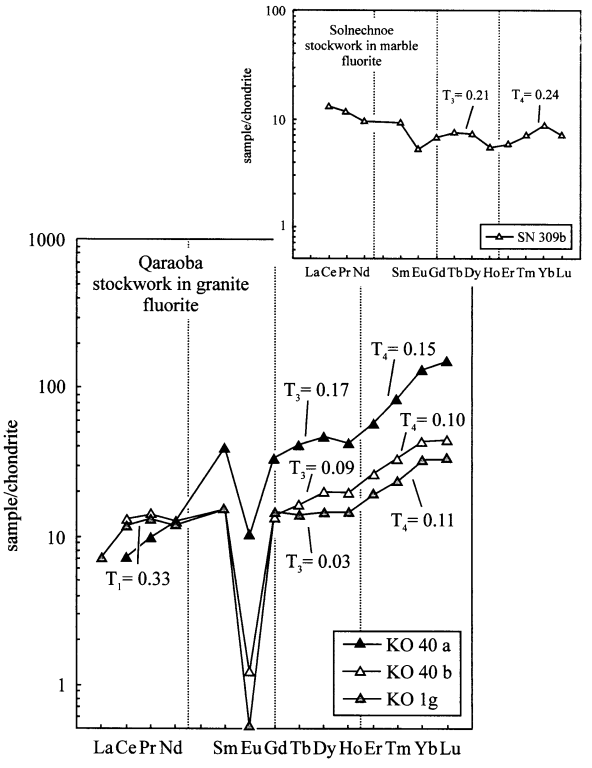

Fig. 6. Chondrite-normalized REE distribution patterns of fluorite from the granite-hosted Qaraoba deposit and the marble-hosted Solnechnoe ore field. The sample KO 40a is the brown core and the sample KO 40b the green rim of a single zoned crystal. The fluorite KO 1g is a green rim surrounding a violet crystal. Both late-stage green samples show pronounced negative Eu anomalies. The brown fluorite SN 309b from the Solnechnoe ore field shows a weak negative Eu anomaly and intense third and fourth tetrads.

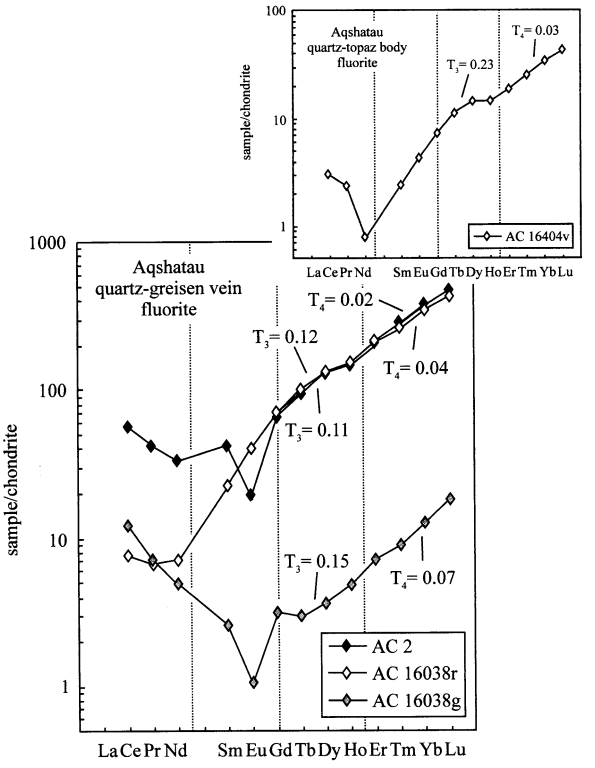

Fig. 7. Chondrite-normalized REE distribution patterns of fluorite samples from the Aqshatau deposit. All samples are characterized by strong $HREE_n$ enrichments and variable Eu anomalies. The negative Eu anomaly is most pronounced in the late-stage sample AC 16038g. Note the similarity between the REE patterns of the rose fluorite (sample AC 16038r) collected from a quartz vein and that of the bluish violet sample taken from a quartz–topaz greisen body (sample AC 16404v).

from the magma–fluid system after phase separation. Analysis of fluorite REE patterns is also advantageous because this mineral occurs frequently in granite-related metal deposits. Moreover, it has been found that the physical and chemical properties of different colored zones within single zoned fluorite aggregates can be used to characterize the evolution of hydrothermal fluids (Jebrak et al., 1985; Constantopoulos, 1988; Trinkler et al., 1993; Morozov et al., 1996; Graupner et al., 1999; Möller and Dulski, 1999; Monecke et al., 2000).

The chemical evolution of the hydrothermal fluid within the endocontact of the Zinnwald deposit can be reconstructed by comparing the lanthanide distribution patterns of the different colored zones of the zoned fluorite aggregate investigated (samples ZW 315/2g and ZW 315/2v) with the REE pattern of the fluorite sampled from the exocontact (sample ZW 379). Fluorite from the endocontact shows an enrichment of the $HREEs_n$ and pronounced negative Eu anomalies whereas fluorite from the exocontact shows an enrichment of the $LREEs_n$ and only a weak negative Eu anomaly (Fig. 5). The Y_n/Dy_n ratio increases from the early stage sample to the later stage samples. Similar evolutionary trends can be observed for the fluorite samples collected in the other rare element deposits. For instance, the brown fluorite core (sample KO 40a) and the green rim (sample KO 40b) of the single fluorite aggregate sampled in the endocontact of the Qaraoba deposit are characterized by strong enrichments of the $HREEs_n$ and pronounced negative Eu anomalies, whereas the exocontact sample (fluorite SN 309b) is characterized by an enrichment of the $LREEs_n$ and a small negative Eu anomaly (Fig. 6). The Y_n/Dy_n ratio in the zoned fluorite aggregate sampled in the endocontact quartz–wolframite vein increased with time. Seifert and Kempe (1994) and Monecke et al. (2000) demonstrated that these systematic changes in lanthanide distribution patterns of fluorite samples can be explained by the chemical evolution of a hydrothermal fluid that initially showed a REE distribution pattern with $HREEs_n > LREEs_n$. The increase of $LREE_n$ concentrations in the fluid with time, and distance from ore-bearing granites, was caused by the uptake of these elements during interaction with $LREEs_n$ enriched wall-rocks. However, the Eu anomalies in the fluorite samples cannot be accounted for by such a process. The Eu content in the fluorite samples is influenced by the interaction of the fluid with the magma as well as Eh and T conditions during fluid migration and fluorite precipitation (Seifert and Kempe, 1994; Goldstein et al., 1995; Kempe and Goldstein, 1997; Monecke et al., 2000). The tetrad effect appears to develop more or less independently from the size of the Eu anomaly and the Y_n/Dy_n ratio in the hydrothermal fluids. The interaction of the fluid with the wall-rocks in the exocontact possibly affected the size of the tetrad effect of individual

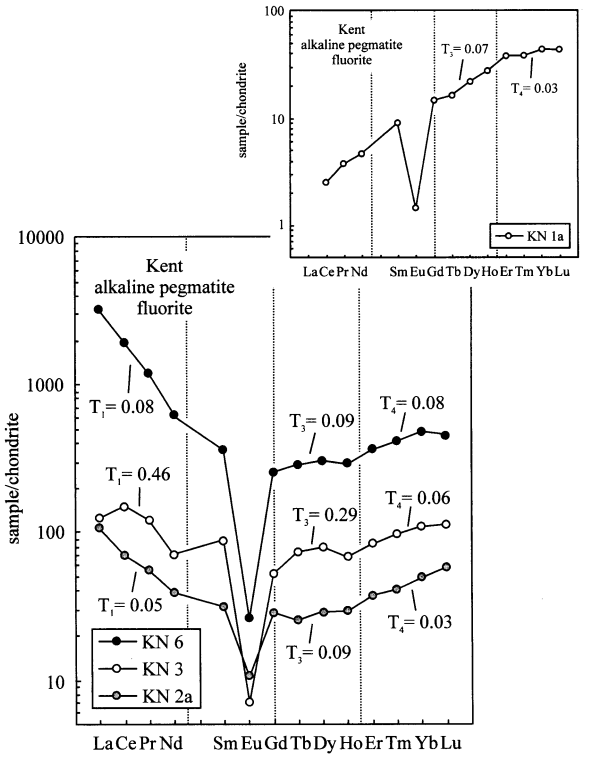

Fig. 8. Chondrite-normalized REE distribution patterns of fluorite sampled from the Kent deposit. The violet sample KN 3 collected from a Zr-Nb mineralized pegmatite body shows a significant tetrad effect, whereas the tetrads in the two green fluorite samples KN 2a and KN 6 are not significant. The colorless sample KN 1a sampled from a barren pegmatite containing optical fluorite exhibits a pronounced $HREE_n$ enrichment.

tetrads and may also have influenced the anomalous enrichment of Y in the fluids.

7. CONCLUSIONS

By use of a quantitative statistical approach, observed tetrad effects have been tested for significance. For whole-rock and fluorite samples derived from magmatic and hydrothermal sources, the appearance of a convex tetrad effect is common, in addition to negative Eu anomalies and nonchondritic Y/Dy ratios. However, no simple correlation was observed between the size of the tetrad effect and the negative Eu anomaly or the extent of Y/Dy fractionation. Therefore, we conclude that these geochemical characteristics developed more or less independently during the ore-forming process.

In contrast to previous suggestions, the convex tetrad effect in whole-rock samples cannot be explained by removal of a respective mirroring concave tetrad effect into a hydrothermal fluid. Hydrothermal precipitates in the endo- and exocontact exhibit only convex tetrad effects. It is argued that the tetrad effect was either a feature of the magma–fluid system before magmatic crystallization or that the tetrad effect in the whole-rock samples was inherited from an external fluid during or after the emplacement of the magma. The size of the tetrad effect in the hydrothermal fluids appears to have decreased with time and also with distance from the ore-bearing granites due to alteration of the wall-rocks. In contrast to the tetrad effect, the anomalous behavior of Eu and Y in the granite-related rare metal systems appears to be related either to processes occurring during the subvolcanic intrusion of the magma–fluid system or to systematic variations in the physico-chemical conditions during fluid migration after the magma–fluid system was split into magma and fluid subsystems.

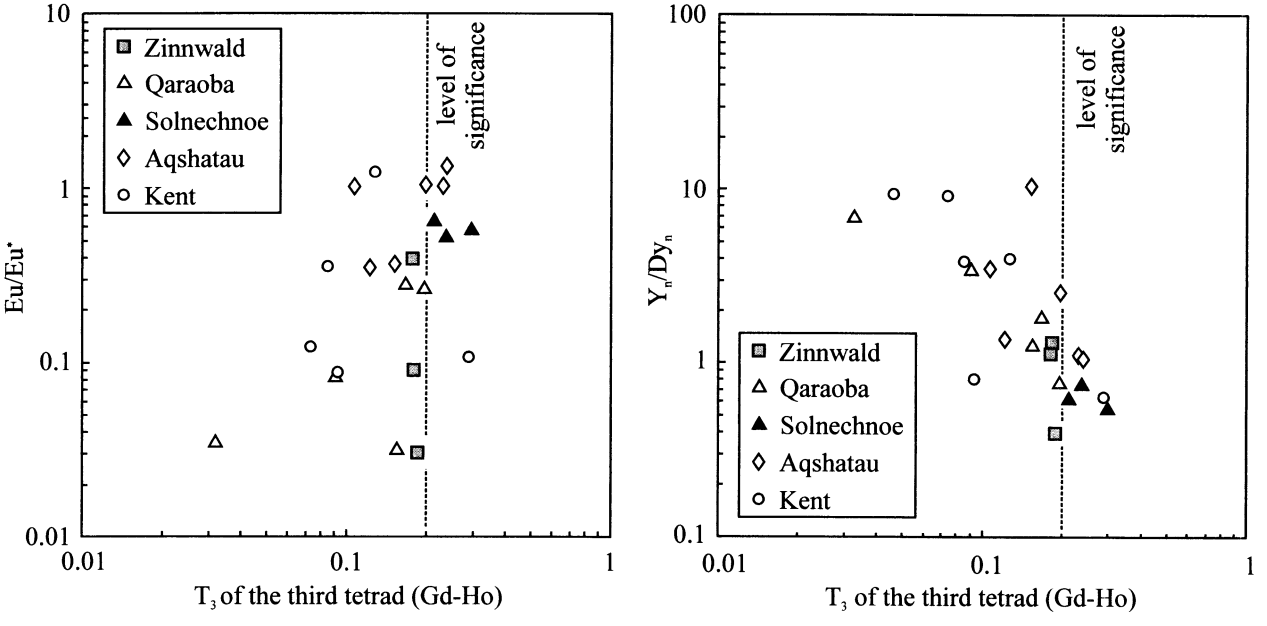

Fig. 9. Diagrams showing the size of the Eu anomalies and the Y_n/Dy_n ratios in the fluorite samples in comparison to the size of the tetrad effect of the third tetrad in the chondrite-normalized REE patterns. No obvious correlation between these geochemical parameters can be observed for the investigated samples.

Acknowledgments—We gratefully acknowledge analytical efforts by B. Düsing, S. Goldstein, W. Klemm, M. Morozov, M. Plötze, and M. Trinkler. Special thanks are extended to P. Dulski for REE analysis of the whole-rock samples from Zinnwald and comments on an earlier version of the manuscript. We are especially grateful to J. Schijf, S. McLennan, R. H. Byrne, and an anonymous reviewer who helped us improve the manuscript. We also express our gratitude for fruitful discussions and comments to P. M. Herzig. L. Panova provided three fluorite samples from Qaraoba and Aqshatau. We appreciate valuable comments on the geology of the Zinnwald tin deposit by R. Seltmann. T.M. gratefully acknowledges financial support provided by the Studienstiftung des Deutschen Volkes. M.S. carried out the investigations on the Zinnwald deposit while in receipt of a DAAD scholarship.

Associate editor: R. H. Byrne

REFERENCES

Ahrens L. H. (1966) Element distributions in specific igneous rocks—VIII. *Geochim. Cosmochim. Acta* **30,** 109–122.

Akagi T., Shabani M. B., and Masuda A. (1993) Lanthanide tetrad effect in kimuraite [$CaY_2(CO_3)_4 \cdot 6H_2O$]: Implication for a new geochemical index. *Geochim. Cosmochim. Acta* **57,** 2899–2905.

Akagi T., Nakai S., and Masuda A. (1998) In-pattern tetrad effect-like variation, so far overlooked, but obviously observed in REE abundances of REE minerals. *Geochem. J.* **32,** 135–141.

Anders E. and Grevesse N. (1989) Abundances of the elements: Meteoritic and solar. *Geochim. Cosmochim. Acta* **53,** 197–214.

Bandurkin G. A. (1964) On the irregular property changes of rare-earth elements [in Russian]. *Geochimija* **1,** 3–15.

Bau M. (1996) Controls on the fractionation of isovalent trace elements in magmatic and aqueous systems: Evidence from Y/Ho, Zr/Hf, and lanthanide tetrad effect. *Contrib. Mineral. Petrol.* **123,** 323–333.

Bau M. (1999) Scavenging of dissolved yttrium and rare earths by precipitating iron oxyhydroxide: Experimental evidence for Ce oxidation, Y-Ho fractionation, and lanthanide tetrad effect. *Geochim. Cosmochim. Acta* **63,** 67–77.

Beskin S. M., Larin V. N., and Marin Yu B. (1996) The greisen Mo-W deposit of Aqshatau, Central Kazakhstan. In *Granite-Related Ore Deposits of Central Kazakhstan and Adjacent Areas* (eds. V. Shatov, R. Seltmann, A. Kremenetsky, B. Lehmann, V. Popov, and P. Ermolov), pp. 145–154. Glagol Publishing.

Cocherie A., Johan V., Rossi P., and Štemprok M. (1991) Trace element variations and lanthanide tetrad effect studied in a Variscan lithium albite granite: Case of the Cinovec granite (Czechoslovakia) [abstract]. In *Source, Transport and Deposition of Metals: Proceedings of an SGA Anniversary Meeting* (eds. M. Pagel and J. L. Leroy), pp. 745–749. Balkema.

Constantopoulos J. (1988) Fluid inclusions and rare earth element geochemistry of fluorite from south-central Idaho. *Econ. Geol.* **83,** 626–636.

Dulski P. (1994) Interferences of oxide, hydroxide and chloride analyte species in the determination of rare earth elements in geological samples by inductively coupled plasma-mass spectrometry. *Fresenius J. Anal. Chem.* **350,** 194–203.

Dulski P. (2001) Reference materials for geochemical studies: New analytical data by ICP-MS and critical discussion of reference values. *Geostand. Newslett.* **25,** 87–125.

Förster H. J. and Tischendorf G. (1994) The western Erzgebirge-Vogtland granites: Implications to the Herzynian magmatism in the Erzgebirge-Fichtelgebirge Anticlinorium [abstract]. In *Metallogeny of Collisional Orogens Focussed on the Erzgebirge and Comparable Metallogenic Settings* (eds. R. Seltmann, H. Kämpf and P. Möller), pp. 35–48. Czech Geological Survey.

Goldstein S. (1997) Geochemische Untersuchungen an Fluoriten und Fergusoniten aus pegmatit- und granitgebundenen Seltenmetallagerstätten. Ph.D. thesis. Freiberg University of Mining and Technology.

Goldstein S., Kempe U., and Klemm W. (1995) REE in fluorite from tin deposits in the Erzgebirge region: Implications for the origin of Eu-anomalies in Li-F granites [abstract]. *Beih. 1 Eur. J. Mineral.* **7,** 85.

Grappin C., Treuil M., Yaman S., and Touray J. C. (1979) Le spèctre des terres rares de la fluorine en tant que marqueur des propriétés du milieu de dépôt et des interactions entre solutions minéralisantes et roches sources. Exemple pris dans le Destrict de la Marche Occidentale (France). *Mineral. Deposita* **14,** 297–309.

Graupner T., Kempe U., Dombon E., Pätzold O., Leeder O., and Spooner E. T. C. (1999) Fluid regime and ore formation in the tungsten(-yttrium) deposits of Kyzyltau (Mongolian Altai): Evidence for fluid variability in tungsten–tin ore systems. *Chem. Geol.* **154,** 21–58.

Höhndorf A., Kämpf H., and Dulski P. (1994) Sm/Nd and Rb/Sr isotopic investigations on fluorite mineralization of the eastern Erzgebirge [abstract]. In *Metallogeny of Collisional Orogens Focussed on the Erzgebirge and Comparable Metallogenic Settings* (eds. R. Seltmann, H. Kämpf and P. Möller), pp. 116–128. Czech Geological Survey.

Irber W. (1999) The lanthanide tetrad effect and its correlation with K/Rb, Eu/Eu*, Sr/Eu, Y/Ho, and Zr/Hf of evolving peraluminous granite suites. *Geochim. Cosmochim. Acta* **63,** 489–508.

Irber W. and Bau M. (1995) Fractionation of Zr/Hf, Y/Ho and the REEs (tetrad effect) and its significance as a geochemical tool for characterization of granite evolution [abstract]. *Beih. 1 Eur. J. Mineral.* **7,** 112.

Jebrak M., Smejkal V., and Albert D. (1985) Rare earth and isotopic geochemistry of the fluorite–barite vein deposits from the western Rouergue District (France). *Econ. Geol.* **80,** 2030–2034.

Jørgensen C. K. (1970) The "Tetrad effect" of Peppard is a variation of the nephelauxetic ratio in the third decimal. *J. Inorg. Nucl. Chem.* **32,** 3127–3128.

Kagi H., Dohmoto Y., Takano S., and Masuda A. (1993) Tetrad effect in lanthanide partitioning between calcium sulfate crystal and its saturated solution. *Chem. Geol.* **107,** 71–82.

Kawabe I. (1992) Lanthanide tetrad effect in the Ln^{3+} ionic radii and refined spin-pairing energy theory. *Geochem. J.* **26,** 309–335.

Kawabe I. (1995) Tetrad effects and fine structures of REE abundance patterns of granitic and rhyolitic rocks: ICP-AES determinations of REE and Y in eight GSJ reference rocks. *Geochem. J.* **29,** 213–230.

Kawabe I. (1996) Convex tetrad effect variations in REE abundances of "North American shale composite" and "Post-Archean Australian average shale." *Geochem. J.* **30,** 149–153.

Kawabe I., Toriumi T., Ohta A., and Miura N. (1998) Monoisotopic REE abundances in seawater and the origin of seawater tetrad effect. *Geochem. J.* **32,** 213–229.

Kempe U. and Goldstein S. (1997) Eu anomalies, tetrad effect and HREE enrichment in fluorites from Sn deposits: Evidence for two source mixing and phase separation [abstract]. *J. Czech Geol. Soc.* **42,** 37.

Lee S. G., Masuda A., and Kim H. S. (1994) An early Proterozoic leuco-granitic gneiss with the REE tetrad phenomenon. *Chem. Geol.* **114,** 59–67.

Liu C. Q., Masuda A., Okada A., Yabuki S., Zhang J., and Fan Z. L. (1993) A geochemical study of loess and desert sand in northern China: Implications for continental crust weathering and composition. *Chem. Geol.* **106,** 359–374.

Luo Y. R. and Byrne R. H. (2000) The ionic strength dependence of rare earth and yttrium fluoride complexation at 25°C. *J. Sol. Chem.* **29,** 1089–1099.

Marchand L., Joseph D., Touray J. C., and Treuil M. (1976) Criteres d'analyse géochimique des gisements de fluorine basés sur l'étude de la distribution des lanthanides — Application au gite de Maine (71-Cordesse, France). *Mineral. Deposita* **11,** 357–379.

Masuda A. and Akagi T. (1989) Lanthanide tetrad effect observed in leucogranites from China. *Geochem. J.* **23,** 245–253.

Masuda A. and Ikeuchi Y. (1979) Lanthanide tetrad effect observed in marine environment. *Geochem. J.* **13,** 19–22.

Masuda A., Kawakami O., Dohmoto Y., and Takenaka T. (1987) Lanthanide tetrad effects in nature: Two mutually opposite types, W and M. *Geochem. J.* **21,** 119–124.

Masuda A., Matsuda N., Minami M., and Yamamoto H. (1994) Approximate estimation of the degree of lanthanide tetrad effect from precise but partially void data measured by isotope dilution and an electron configuration model to explain the tetrad phenomenon. *Proc. Jpn. Acad.* **70B,** 169–174.

McLennan S. M. (1994) Rare earth element geochemistry and the "tetrad" effect. *Geochim. Cosmochim. Acta* **58,** 2025–2033.

Minami M. and Masuda A. (1997) Approximate estimation of the degree of lanthanide tetrad effect from the data potentially involving all lanthanides. *Geochem. J.* **31,** 125–133.

Möller P. and Dulski P. (1999) LA-ICPMS study of REE and Y distribution in fluorite [abstract]. In *Mineral Deposits: Processes to Processing. Proceedings of the 5th Biennial SGA Meeting and the 10th Quadrennial IAGOD Symposium* (eds. C. J. Stanley et al.), pp. 1133–1136. Balkema.

Monecke T., Monecke J., Mönch W., and Kempe U. (2000) Mathematical analysis of rare earth element patterns of fluorites from the Ehrenfriedersdorf tin deposit, Germany: Evidence for a hydrothermal mixing process of lanthanides from two different sources. *Mineral. Petrol.* **70,** 235–256.

Morozov M., Trinkler M., Plötze M., and Kempe U. (1996) Spectroscopic studies on fluorites from Li-F and alkaline granitic systems in Central Kazakhstan. In *Granite-Related Ore Deposits of Central Kazakhstan and Adjacent Areas* (eds. V. Shatov, R. Seltmann, A. Kremenetsky, B. Lehmann, V. Popov, and P. Ermolov), pp. 359–369. Glagol Publishing.

Münker C. (1998) Nb/Ta fractionation in a Cambrian arc/back arc system, New Zealand: Source constraints and application of refined ICPMS techniques. *Chem. Geol.* **144,** 23–45.

Nugent L. J. (1970) Theory of the tetrad effect in the lanthanide(III) and actinide(III) series. *J. Inorg. Nucl. Chem.* **32,** 3485–3491.

Peppard D. F., Mason G. W., and Lewey S. (1969) A tetrad effect in the liquid–liquid extraction ordering of lanthanides (III). *J. Inorg. Nucl. Chem.* **31,** 2271–2272.

Robinson P., Townsend A. T., Yu Z., and Münker C. (1999) Determination of scandium, yttrium and rare earth elements in rocks by high resolution inductively coupled plasma-mass spectrometry. *Geostand. Newslett.* **23,** 31–46.

Rub A. K., Štemprok M., and Rub M. G. (1998) Tantalum mineralization in the apical part of the Cínovec (Zinnwald) granite stock. *Mineral. Petrol.* **63,** 199–222.

Schijf J. and Byrne R. H. (1999) Determination of stability constants for the mono- and difluoro-complexes of Y and the REE, using cation-exchange resin and ICP-MS. *Polyhedron* **18,** 2839–2844.

Seifert Th. and Kempe U. (1994) Sn-W-Lagerstätten und spätvariszische Magmatite des Erzgebirges. *Beih. 2 Eur. J. Mineral.* **6,** 125–172.

Siekierski S. (1971) The shape of lanthanide contraction as reflected in the changes of the unit cell volumes, lanthanide radius and the free energy of complex formation. *J. Inorg. Nucl. Chem.* **33,** 377–386.

Štemprok M. (1967) Genetische Probleme der Zinn-Wolfram Vererzung im Erzgebirge. *Mineral. Dep.* **2**, 102–118.

Štemprok M. and Šulcek Z. (1969) Geochemical profile through an ore-bearing lithium granite. *Econ. Geol.* **64**, 392–404.

Trinkler M., Kempe U., Plötze M., and Rieser U. (1993) Über rosa und braunen Fluorit aus Sn-W-Lagerstätten. *Chem. Erde.* **53,** 165–181.

Watkins P. J. and Nolan J. (1992) Determination of rare-earth elements, yttrium, scandium and hafnium using cation-exchange separation and inductively coupled plasma-atomic emission spectrometry. *Chem. Geol.* **95,** 131–139.

Yu Z., Robinson P., Townsend A. T., Münker C., and Crawford A. J. (2000) Determination of high field strength elements, Rb, Sr, Mo, Sb, Cs, Tl and Bi at ng g^{-1} levels in geological reference materials by magnetic sector ICP-MS after HF/$HClO_4$ high pressure digestion. *Geostand. Newslett.* **24,** 39–50.

Yurimoto H., Duke E. F., Papike J. J., and Shearer C. K. (1990) Are discontinuous chondrite-normalized REE patterns in pegmatitic granite systems the results of monazite fractionation? *Geochim. Cosmochim. Acta* **54,** 2141–2145.

Zakharchenko A. I., Moskalyuk A. A., Gurevich M. G., and Ovchinnikov I. M. (1968) Temperature and composition of fluids during formation of fluorite-quartz veins, greisen, and pegmatites within the Kent granite massif [in Russian]. *Trudy Vsesoyuznogo Nauchno-issledovatel'skogo Instituta Sinteza Mineral'nogo Syrýa* **9,** 59–74.